THE JOURNAL OF PHYSICAL CHEMISTRY B

B: Biophysics; Physical Chemistry of Biological Systems and Biomolecules

Molecular Origin of the Elastic State of Aqueous Hyaluronic Acid

Giulia Giubertoni, Federica Burla, Cristina Martinez-Torres, Biplab Dutta, Galja Pletikapi#, Eddie G. Pelan, Yves L. A. Rezus, Gijsje H. Koenderink, and Huib J. Bakker

J. Phys. Chem. B, **Just Accepted Manuscript** • DOI: 10.1021/acs.jpcb.9b00982 • Publication Date (Web): 19 Mar 2019

Molecular Origin of the Elastic State of Aqueous Hyaluronic Acid

Giulia Giubertoni [†], Federica Burla [†], Cristina Martinez-Torres [†], Biplab Dutta [†], Galja Pletikapic [†], Eddie Pelan [‡], Yves L.A. Rezus [†], Gijsje H. Koenderink [†,], and Huib J. Bakker [†,*]*

[†] AMOLF, Science Park 104, 1098 XG Amsterdam, The Netherlands

[‡] Unilever Research and Development Vlaardingen B.V, Olivier van Noortlaan 120, Vlaardingen, 3133 AT, The Netherlands

Corresponding authors

[*]Gijsje H. Koenderink, and Huib J. Bakker

G.Koenderink@amolf.nl, H.Bakker@amolf.nl

Abstract:

The macroscopic mechanical properties of biological hydrogels are broadly studied and successfully mimicked in synthetic materials, but little is known about the molecular interactions that mediate these properties. Here we use two-dimensional infrared spectroscopy (2D-IR) to study the pH-induced gelation of hyaluronic acid, a ubiquitous biopolymer, which undergoes a transition from a viscous to an elastic state in a narrow pH range around 2.5. We find that the gelation originates from the enhanced formation of strong inter-chain connections, consisting of a double amide-COOH hydrogen-bond and an N-D-COO- hydrogen-bond on the adjacent sugars of the hyaluronan disaccharide unit. We confirm the enhanced inter-chain connectivity in the elastic state by AFM imaging.

Introduction

Hydrogels regulate the mechanical properties of cells and tissues and thereby play an important role in many biological and pathophysiological processes, ranging from stem cell differentiation and the degradation of aging cartilage to wound healing [1–6]. An important feature of natural hydrogels is their ability to tune their viscoelastic properties in response to environmental stimuli such as the solution pH, temperature and salt conditions. Up to now, it has been difficult to connect the macroscopic response of hydrogels to the underlying molecular interactions, e.g. hydrogen-bond and hydrophobic interactions, thus limiting the capability to predict and tune the properties of hydrogels.

One of the few techniques able to track interactions at the molecular scale is two-dimensional infrared spectroscopy (2D-IR).[7] 2D-IR shares with two-dimensional nuclear magnetic resonance (2D-NMR) the ability to resolve molecular couplings and dynamics, but 2D-IR can resolve these interactions at a much shorter time scale. Molecular interactions such as hydrogen-bonds or electrostatic forces usually change on a time scale of picoseconds, and with 2D-IR snapshots of these interactions can be taken with femtosecond time resolution[8].

Here we use 2D-IR to identify the molecular interactions that drive the pH-triggered gelation of hyaluronic acid, a natural polyelectrolyte that has received widespread attention, being one of the main components of the extracellular matrix. It is important for cell-cell communication and also plays an important role in many biological processes such as joint lubrication, skin hydration and cell migration[9], while its dysregulation contributes to cancer development[10]. Due to its biocompatibility, hyaluronic acid is also widely used as a scaffold for cell culture and drug delivery[11–15]. Hyaluronic acid is a paradigmatic example of a responsive natural hydrogel: it displays a sharp transition in mechanical behavior at pH 2.5, switching from a viscous state to an elastic gel denoted as the '*putty state*'[16]. The mechanism underlying this remarkable liquid-to-gel transition has been investigated for over almost a century with macroscopic techniques that map the dependence of the viscoelastic properties on pH, temperature and ionic strength[17–19]. Based on these studies, it has been proposed that at pH=2.5, the net charge of the polyelectrolyte chains may be sufficiently suppressed to enable the formation of inter-chain hydrogen-bond interactions that would act as crosslinks[20–26]. This principle was suggested to be applicable to the wider class of polysaccharides [27], but there has been no direct evidence for this putative pH-triggered hydrogen-bonding mechanism.

Experimental Section

Sample preparation

The samples were prepared in a glass vial by adding water (or heavy water), NaCl (0.15 M) and HCl (or DCl) to achieve different molarities ranging from 0 to 80 mM of acid. All these chemicals were provided by Sigma Aldrich. A specific amount of hyaluronic acid sodium salt in powder form from Streptococcus equii bacterial from Sigma Aldrich (M_w>1Mda), or from Lifecore Biomedical (M_w~100kDa) was added to the solution to reach a final concentration ranging from 10 to 20 mg/ml. The samples were left to equilibrate at room temperature for at least 24 hours before measuring. Samples were stored for at most 1 week at a temperature of 4 °C, to slow down hydrolytic degradation process.

Rheology

Rheology measurements were performed with a stress-controlled rheometer (Anton Paar MCR 501) equipped with stainless steel parallel plates with a diameter of 40 mm. The experiments were performed at a gap size of 100 μm and at a temperature of 22°C set by a Peltier system. Samples left to equilibrate for one week to reach homogeneity were loaded on the plate using a spatula. After thermal equilibration, the elastic and viscous shear moduli were probed by performing oscillatory shear measurements at an oscillation frequency of 0.5 Hz and a strain amplitude of 0.5%, which is well within the linear

viscoelastic regime for hyaluronan. The reported results are averages of at least three measurements for each pH. For each sample, the pH was measured using a pH meter (Hanna Instruments).

FTIR

All linear absorption measurements were performed using a Bruker Vertex 80v FTIR spectrometer equipped with a liquid-nitrogen-cooled-mercury-cadmium-telluride (MCT) detector. The spectra were recorded under nitrogen atmosphere at a wavelength resolution of 3 cm^{-1}. For every spectrum 100 scans were averaged. In all the measurements, a standard sample cell with a path length of 100 or 75 μm was used. The reported spectra were corrected for the absorption of the solvent background.

2DIR

In the 2DIR experiments, we perform one color experiments by pumping and probing around 1680 cm^{-1} and two color experiments by pumping at 1680 cm^{-1} and probing at 1450 cm^{-1}. The home-built setup that we use has been described before [28]. The excitation is performed with a pair of femtosecond mid-infrared pulses. This excitation pulse-pair induces transient absorption changes, which are monitored by a probe pulse that is delayed by a time T_w. After transmission through the sample, the probe pulse is sent into an infrared spectrograph and detected with an infrared mercury-cadmium-telluride (MCT) detector array, thus yielding the transient absorption spectrum as a function of the probe frequency. The dependence of the transient absoption spectrum on the excitation frequency is determined by measuring transient spectra for many different delay times between the two excitation pulses. By Fourier transformation of these spectra, we obtain the dependence of the transient absorption spectrum on the excitation frequency. By plotting the transient absorption spectrum as a function of the excitation and the probing frequency, we obtain a two-dimensional infrared (2D-IR) transient absorption spectrum for each delay time T_w.

AFM imaging

For the AFM measurements, freshly cleaved mica was briefly rinsed with 0.15 M NaCl before sample deposition. 50 μL of 100 mg/l HA solution were then deposed and left to adsorb for 15 min. The mica was then rinsed with ultra-pure water and dried at room temperature. Imaging was performed using tapping mode in air with a TAP150 cantilever on a Veeco Dimension 3100 AFM. The scanning rate was set to 0.5 Hz, with a scan resolution of 512x512. To retrieve the filament height values, the AFM height images were processed using the open-source software Gwyddion[29] to correct for tilt in the image, and the transversal profiles corresponding to the filament cross-section were taken. Using a custom script on MATLAB, each profile was corrected for the background noise, and the values of all the local maxima were pooled together to obtain a height distribution for each condition tested.

Results

Rheology and Infrared Spectroscopy

Hyaluronic acid has a relatively simple linear structure and homogeneous composition with repeating disaccharides composed of N-acetyl-glucosamine and glucuronic-acid (illustrated in the inset of Fig. 1b). The pH-dependent viscoelastic behavior of hyaluronic acid solutions stands out clearly in tube inversion assays, as shown in Fig. 1a. While the sample prepared in a solution state ("s") at pH 1.6 readily flows, the sample prepared in the "putty state" ("p") at pH 2.5 only flows on a time scale of minutes. This large difference in time scales originates from a pH-triggered transition in rheological properties from liquid to gel. To study the pH dependence of this transition in quantitative detail, we performed rheological experiments on semi-dilute solutions of high and low molecular weight hyaluronic acid. We studied solutions in heavy water (D_2O), since heavy water is used as a solvent in 2D-IR studies of the amide and carbonyl vibrations. 2D-IR cannot be applied to solutions in H_2O, as the amide and carbonyl

vibrations of hyaluronic acid absorb in the same infrared frequency region as the bending vibration of H_2O (between 1600 and 1700 cm^{-1}). In all experiments, the pD values are converted to pH values[30] (see SI Appendix). Fig. 1b shows that the elastic and the viscous moduli sharply increase in a narrow range around a pH of 2.5, revealing a liquid-gel transition. This transition occurs at a pH value just below the pK_a, which is about 2.9[12,18,25]. We find a quantitatively similar pH dependence of the viscous and elastic moduli for hyaluronan solutions in H_2O (see Supplementary Appendix, Fig. S2), which shows that the isotope composition of the solvent has a negligible effect on the mechanical properties.

We studied the protonation state of hyaluronan as a function of pH with linear IR spectroscopy (Fig.1c). The relative intensities of the carboxylic acid and carboxylate anion bands of hyaluronan directly reflect the protonation state of hyaluronan.The anti-symmetric vibration of the carboxylate anion, ν_{ant,COO^-} absorbs at 1607 cm^{-1}, and the amide I band, $\nu_{AM.I}$ absorbs at 1633 cm^{-1}. The C=O vibration of the COOD group, that will be denoted as ν_{COOD}, absorbs around 1726 cm^{-1}. At pH = 2.5, the COO^- and COOD groups are present in a ratio of 1:4 (inset in Fig.1c), which corresponds to a pK_a of 2.9, as reported in literature[12].

Two Dimensional-Infrared spectroscopy

We use 2D-IR spectroscopy to study the intermolecular interactions among hyaluronic acid chains that lead to the sol-gel transition. We excite the amide and the carboxyl vibrations with a strong femtosecond infrared pulse pair (~100 fs, 4 μJ per pulse). This excitation induces transient absorption changes that are probed with a weaker (0.35 μJ) single femtosecond probing pulse that is delayed by a time T_w. The excitation and probe pulses are centered at 1680 cm^{-1} with a bandwidth of 200 cm^{-1}. The excitation and probe spectra thus have sufficient spectral width to cover the ν=0 to ν=1 transition (*bleach*) and the ν=1 to ν=2 transition (excited state absorption, or *esa*) of the ν_{ant,COO^-}, the ν_{COOD}, and the $\nu_{AM.I}$ vibrations.

Fig.2a and Fig.2b compare the 2D-IR spectra measured for the solution (pH=1.6) and the putty state (pH=2.5), both for T_w =1.5 ps**.** Bleaching (increased transmission) is indicated in blue, while increased absorption (*esa*) is indicated in red. The bleach of the ν=0 to ν=1 transition, and the *esa* of the $\nu_{AM.I}$ are centered at 1639 cm^{-1} and 1619 cm^{-1}, respectively, along the probe frequency axis, while for the ν_{COOD} these signals are centred at 1731 cm^{-1} and 1703 cm^{-1}, respectively (see also Supplementary Appendix, Table S2). The bleaching and *esa* of the ν_{ant,COO^-} mode are in the low-frequency wing of the bleaching and *esa* of the amide I vibration, and lead to an elongation of the bleaching and the induced absorption signals to the lower-left corner of the 2D-IR spectrum. We observe additional signals in the off-diagonal regions of the 2D-IR spectrum, indicating that the carboxyl and amide modes are coupled. In the upper pump-frequency region, the cross-peak signal represents the effect of the excitation of the ν_{COOD} vibration on the spectrum of the $\nu_{AM.I}$ mode. In the lower pump-frequency region, the spectral shape of the carboxylic acid vibration is elongated along the pump axis (Fig.S7). This effect reduces the visibility of the upward cross-peak, which represents the effect of the excitation of the $\nu_{AM.I}$ vibration on the spectrum of the ν_{COOD} vibration. For this reason, we focus our analysis on the downward cross-peak that represents the effect of the excitation of the carboxylic acid vibration on the $\nu_{AM.I}$ vibration. The excitation of the ν_{COOD} vibration also leads to a cross-peak signal with the amide II mode ($\nu_{AM.II}$) at1490 cm^{-1}. This signal results from the excitation of low-frequency modes following the relaxation of the ν_{COOD} mode. The excitation of these low-frequency modes affects the absorption specta of both the ν_{COOD} and $\nu_{AM.II}$ modes (see SI Appendix, Fig.S6a-b).

To learn more about the mechanism that underlies the cross-peak signals of the amide I modes following excitation of the COOD vibration, we compare the dependence on time delay for the solution and the putty states (Fig. 3a). We normalized the transients to the bleaching signal of the carboxylic acid vibration at early time delay (~0.2 ps). From ~1.5 ps on, the decay of the transients is quite similar to that of the ν_{COOD} - $\nu_{AM.II}$ cross-peak, showing a time constant of ~3 ps. However, the transients of the ν_{COOD} - $\nu_{AM.I}$ cross-peak signals have their maximum at 0.3-0.5 ps, a much earlier delay time than the one observed for the ν_{COOD} - $\nu_{AM.II}$ cross-peak (~1-1.5 ps). In addition, the transients of the ν_{COOD} - $\nu_{AM.I}$ cross-peak show an additional faster decay component with a time constant of ~0.6 ps. Interestingly, the transient of the ν_{COOD} - $\nu_{AM.I}$ cross-peaks has a much higher intensity at early delay times for the putty state than for the solution state. This observation, together with the dynamics observed for the ν_{COOD} - $\nu_{AM.II}$ cross-peak, indicates that the ν_{COOD} - $\nu_{AM.I}$ cross-peak signal contains contributions from two distinct mechanisms: 1) energy transfer from the excited COOD vibration to the amide I vibration; 2) anharmonic coupling to low-frequency modes that affect the vibrational spectrum of the amide I mode. The relaxation model corresponding to these two mechanisms is illustrated in Fig.3b.

The cross-peak signal arising from the energy transfer rises with a time constant T_{ent}, representing the time scale of energy transfer from the excited COOD vibration to the accepting amide I vibration, and decays with the vibrational lifetime $T_{1AM.I}$ of the amide I vibration. This direct energy transfer does not occur for the amide II mode because there is a rather large energy difference between the ν_{COOD} and $\nu_{AM.II}$ vibrations. We extract the value of $T_{1AM.I}$ from the diagonal signal of the amide I mode in the 2D-IR spectrum. We find that $T_{1AM.I}$ is comparable to the vibrational lifetime of the COOD vibration: $T_{1AM.I}$ = 0.65±0.1 ps. The time constants of the second mechanism involving anharmonic coupling to low-frequency modes can be extracted from a fit to the transient of the ν_{COOD} - $\nu_{AM.II}$ cross-peak (SI Appendix, Fig.S6b). We thus fit the transients of the ν_{COOD} - $\nu_{AM.I}$ cross-peak to the following expression containing the lifetimes of the COOD vibration, T_{1COOD}, the amide I vibration, $T_{1AM,I}$, and the low-frequency-modes, T_{1LFM}:

$$\frac{\Delta\alpha_{CP}(t)}{\Delta\alpha_{COOD}(\bar{t})} = \boldsymbol{c_{anh}}\left(\frac{T_{1LFM}}{T_{1COOD}-T_{1LFM}}\right)\left(e^{-t/T_{1COOD}}-e^{-t/T_{1LFM}}\right)+\boldsymbol{c_{ent}}\left(\frac{T_{1AM.I}}{\boldsymbol{T_{ent}}-T_{1AM.I}}\right)\left(e^{-t/\boldsymbol{T_{ent}}}-e^{-t/T_{1AM.I}}\right)$$

Eq. 1

Here $\frac{\Delta\alpha_{cp}(t)}{\Delta\alpha_{COOD}(\bar{t})}$ is the intensity of the cross-peak normalized to the intensity of the ν_{COOD} vibration at early time delay, $\bar{t} = 200\,fs$. The parameters $\boldsymbol{c_{anh}}$ and $\boldsymbol{c_{ent}}$ represent the cross-peak amplitudes associated with the anharmonic coupling and direct energy transfer mechanisms, respectively. $\boldsymbol{T_{ent}}$,$\boldsymbol{c_{anh}}$ and $\boldsymbol{c_{ent}}$ are the only free parameters. As shown in Fig.3a, $\boldsymbol{c_{ent}}$ is nearly twofold larger for the putty state than for the solution state, whereas $\boldsymbol{c_{anh}}$ is comparable for the two states. For the time constant $\boldsymbol{T_{ent}}$ we obtain a value of 150 ±50 fs. The energy transfer to the amide I mode constitutes an additional channel for vibrational relaxation of the COOD mode. The fact that we do not observe a significant difference in T_{1COOD} between the putty and the solution state indicates that this energy transfer process only occurs for a minor fraction of

the COOD groups. From the values of c_{ent}, we estimate this fraction to be 13±2% for the putty state and 7±2% for the solution state. The time constant T_{ent} also does not change upon the formation of the putty state which shows that the efficiency of the energy transfer remains the same. Hence, upon formation of the putty state only the number of COOD groups showing energy transfer increases.

The ultrafast energy transfer between the C=O vibration of the COOD group and the amide I vibration of the amide group can be well explained from the presence of a hydrogen bond between the COOD and the amide groups [31]. To get more information on the nature of this hydrogen bond, we compared the intensity of the ν_{COOD}-$\nu_{AM.I}$ cross-peak signal for polarizations of the probing pulse parallel and perpendicular to the polarization of the excitation pulse. The ratio of these two signals reveals the relative orientation of the transition dipole moments of the excited and probed vibrations that form the cross-peak signal[32]. From the ratio of the signals at T_w between 0.3 and 1 ps (where the energy transfer mechanism is predominant), we find that the angle between the transition dipoles of ν_{COOD} and $\nu_{AM.I}$ is ~20 (SI Appendix, Fig. S9). As the transition dipole moment of $\nu_{AM.I}$ is at an angle of 20 relative to the C=O bond of the amide group[33], we conclude that the hydrogen-bond configuration involves a parallel (or anti-parallel) alignment between the C=O groups of the carboxylic acid and amide, forming two closely spaced intermolecular hydrogen bonds between the amide and carboxylic acid groups, i.e. C=O-OD...O=C-ND and -N-D...O=C-OD...O=C-. This geometry, in which the amide and carboxylic acid groups act both as hydrogen-bond donor and acceptor stabilizing the hydrogen-bonded structure formed by these two molecular groups, constitutes a strong inter-chain connection. We conclude that the putty state at pH=2.5 contains a two-fold higher density of these strong double hydrogen-bonds than the solution state at pH=1.6.

To study the role of the COO^- groups in the formation of the putty state, we also measure 2DIR spectra where we excite and probe the ν_{ant,COO^-} and the $\nu_{AM.I}$ vibrations. Since the absorption bands of these two vibrations overlap, we subtract the parallel signal from three times the perpendicular signal. In the resulting difference spectrum, the diagonal peaks are strongly suppressed since the corresponding parallel signal is ~3 times larger than the perpendicular signal. This procedure is thus ideally suited to reveal the presence of cross-peak signals of vibrations that are differently oriented. This strategy has been extensively used in 2DIR experiments on proteins to resolve vibrational couplings[34]. Fig. 4a reports the resulting difference 2DIR spectrum at pH= 2.5 (putty state). On the diagonal, we observe some residual signal due to orientational relaxation of the COO^- and amide molecular groups.[35–37] In addition, we also see clear off-diagonal signals (indicated by the yellow rectangles). In Figure 4b we plot the transient absorption spectrum at pH=2.5 (black cirkles) obtained from Fig. 4a by averaging the signals with pump frequencies between 1600 and 1620 cm^{-1}, corresponding to the excitation of the ν_{ant,COO^-} vibration. The resulting spectrum is compared with the transient absorption spectrum at pH=2.9 that is obtained using the same procedure (SI Appendix, Fig. S12). The transient absorption spectrum at pH 2.5 clearly shows an enhanced absorption signal around the amide I vibrational frequency, which implies that excitation of the ν_{ant,COO^-} vibration yields an enhanced response of the $\nu_{AM.I}$ vibration at pH=2.5. This means that in the putty state (*pH=2.5*) the interaction between the COO^- and amide molecular groups is enhanced. A similar enhancement is observed for the other cross-peak signal, i.e. exciting the amide I vibration and probing the COO^- mode (SI Appendix, Fig. S11f). Hence, our results show that the formation of single N-D-COO^- hydrogen bonds is enhanced in the putty state, in addition to the enhanced presence of double amide-COOH hydrogen-bonds in this state.

Atomic Force Spectroscopy (AFM)

We also perform atomic force microscopy (AFM) imaging of hyaluronic acid solutions at different pH values to investigate to what extent the additional hydrogen bonds in the putty state are formed within or between hyaluronic acid chains (Fig.5a,b). At pH=7 we mainly observe pearl-necklace conformations: thin chains alternating with thicker globular configurations. The globular portions are likely due to the low affinity for mica[38]. At pH=2.5 the AFM images clearly show a much larger density of thick filaments than at pH=7, indicative of inter-chain interactions. To quantify the extent of lateral association of hyaluronan polymers, we measured the heights of the filaments at pH=7 and pH=2.5 (Fig.5c). At neutral pH, we find a Gaussian height distribution centered at an average filament height h_0=0.37 nm. This value is consistent with the expected thickness of a single hyaluronan chain[38]. At pH=2.5 we find a much broader distribution, and h_0=0.53 nm, meaning that the filaments are thicker. Since the length of the filaments at pH=2.5 is not changed compared with pH=7, we conclude that this thickening is mainly due to enhanced inter-chain interactions that laterally associate the strands.

Discussion

The two-dimensional infrared (2D-IR) spectroscopy measurements show that the remarkable pH-triggered gelation of hyaluronic acid at pH 2.5 involves the enhanced formation of double hydrogen bonds between carboxylic acid and amide groups, and of strong single hydrogen bonds between carboxylate anion (which is a stronger hydrogen-bond acceptor) and amide groups. The enhanced formation of hydrogen bonds is intimately related and even enabled by changes in the structure and electrostatic interactions of the hyaluronan polymer chains.

An important question is why the gelation only occurs in a narrow pH range. In particular, one may wonder why the gelation does not occur for a larger pH range below 2.5, as at lower pH there will be even more carboxylic acid groups and thus potentially even more strong double hydrogen bonds with the amide groups located on a different chain.

The answer to this question can be found in the special structure of the hyaluronic acid disaccharide unit, which contains a carboxylic acid group and an amide group on neighboring sugar units (see inset of Fig.1b). The formation of a double amide-carboxylic acid hydrogen-bond structure involves a quite strict local positioning of the hyaluronic acid chains, which prevents the formation of a second double hydrogen-bond structure at the adjacent saccharide units. Hence, the following mechanistic picture arises (Fig. 6): at pH=2.5, the partial deprotonation of the carboxylic acid groups allows for a high probability of forming a strong double amide-COOH hydrogen-bond (green box) and an adjacent strong N-D-COO- hydrogen bond (orange box), together forming a very strong inter-chain connection. In the single N-D-COO^- hydrogen bond, the N-D of an amide group acts as the hydrogen bond donor and the COO- anion group as the hydrogen-bond acceptor. For a sufficient length and concentration of the hyaluronic acid chains, this enhanced hydrogen-bond formation will yield a long-range connected network that behaves as an elastic solid, the putty state. This state is not formed at lower pH, because at these pH values very few carboxylic acid groups are deprotonated and the strong double amide-COOH hydrogen-bond can only be combined with a relatively weak single N-D-COOH or single COOH-amide hydrogen bond on the neighboring sugar units, thus forming a weaker inter-chain connection. As a result, less inter-chain connections are formed (ca. two-fold less at pH=1.6) and the overall connectivity is too low to form an elastic gel. At pH values above 2.5, the putty state is also not formed, because a large fraction of the carboxylic acid groups is deprotonated, which implies that no double amide-COOH hydrogen-bonds can be formed. In addition, Coulomb repulsion will prevent the formation of N-D…-O-C hydrogen

bonds on neighboring sugar units. As a result, the density of inter-chain connections is again too low to allow for gel formation.

Conclusions

In summary, we studied the molecular origin of the 'putty state' of the biologically important polysaccharide hyaluronic acid, which undergoes a sol-gel transformation only in a narrow range around pH=2.5. Using two-dimensional infrared (2D-IR) spectroscopy, we find that this remarkable transition is accompanied by the enhanced formation of strong inter-chain connections that consist of a strong double amide-COOH hydrogen-bond (green box in Figure 6) and a strong N-D-COO- hydrogen bond (orange box in Figure 6) on the adjacent sugar groups of the hyaluronan disaccharide unit. These strong collective inter-chain connections can only form when the carboxylic acid groups are partially deprotonated, which explains why the putty state is observed in a narrow pH range only. The enhanced inter-chain connectivity in the putty state is confirmed by AFM measurements that reveal the association of hyaluronan into thick strands in this state.

The present study illustrates that the combination of 2D-IR spectroscopy, AFM and rheology constitutes a unique tool to identify the molecular mechanisms by which hydrogels respond to environmental stimuli. This combined multiscale approach has great potential to investigate the molecular origin of the biological functionalities of other natural polyelectrolytes, and to assist in the rational design of supramolecular biomaterials with life-like functionalities[14].

Acknowledgements: This work is part of the industrial partnership programme Hybrid Soft Materials that is carried out under an agreement between Unilever Research and the Netherlands Organisation for Scientific Research (NWO). The authors wish to thank Lukas Helmbrecht for making the photographs.

Supporting Information Available: Data Analysis Methods; Hyaluronic acid gel pictures; Rheology Experiments in Water; Linear Infrared Spectra; Anisotropy data; 2D-IR spectra; AFM measurements. This information is available free of charge via the Internet at http://pubs.acs.org.

Author Information:

Corresponding Authors:

*email:H.Bakker@amolf.nl; G.Koenderink@amolf.nl

ORCID:

G.Giubertoni: **0000-0002-3417-4987**

F.Burla: **0000-0002-4491-0589**

G.H.Koenderink: **0000-0002-7823-8807**

H.J.Bakker: **0000-0003-1564-5314**

Notes: The authors declare no competing financial interests

REFERENCES

(1) Chaudhuri, O.; Gu, L.; Klumpers, D.; Darnell, M.; Bencherif, S. A.; Weaver, J. C.; Huebsch, N.; Lee, H.; Lippens, E.; Duda, G. N.; et al. Hydrogels with Tunable Stress Relaxation Regulate

Stem Cell Fate and Activity. *Nat. Mater.* **2016**, *15* (3), 326–334.

(2) Engler, A. J.; Sen, S.; Sweeney, H. L.; Discher, D. E. Matrix Elasticity Directs Stem Cell Lineage Specification. *Cell* **2006**, *126* (4), 677–689.

(3) Vining, K. H.; Mooney, D. J. Mechanical Forces Direct Stem Cell Behaviour in Development and Regeneration. *Nature Reviews Molecular Cell Biology*. Nature Publishing Group November 8, 2017, pp 728–742.

(4) Lee, H.; Gu, L.; Mooney, D. J.; Levenston, M. E.; Chaudhuri, O. Mechanical Confinement Regulates Cartilage Matrix Formation by Chondrocytes. *Nat. Mater.* **2017**, *16* (12), 1243–1251.

(5) Green, J. J.; Elisseeff, J. H. Mimicking Biological Functionality with Polymers for Biomedical Applications. *Nature*. 2016.

(6) Rosales, A. M.; Anseth, K. S. The Design of Reversible Hydrogels to Capture Extracellular Matrix Dynamics. *Nat. Rev. Mater.* **2016**, *1* (2), 15012.

(7) P.Hamm; M.Zanni. *Concepts and Methods of 2D Infrared Spectroscopy*; Cambridge University Press, 2011.

(8) Kolano, C.; Helbing, J.; Kozinski, M.; Sander, W.; Hamm, P. Watching Hydrogen-Bond Dynamics in a β-Turn by Transient Two-Dimensional Infrared Spectroscopy. *Nature* **2006**, *444* (7118), 469–472.

(9) Kogan, G.; Šoltés, L.; Stern, R.; Gemeiner, P. Hyaluronic Acid: A Natural Biopolymer with a Broad Range of Biomedical and Industrial Applications. *Biotechnol. Lett.* **2006**, *29* (1), 17–25.

(10) Tian, X.; Azpurua, J.; Hine, C.; Vaidya, A.; Myakishev-Rempel, M.; Ablaeva, J.; Mao, Z.; Nevo, E.; Gorbunova, V.; Seluanov, A. High-Molecular-Mass Hyaluronan Mediates the Cancer Resistance of the Naked Mole Rat. *Nature* **2013**, *499* (7458), 346–349.

(11) Singh, A.; Corvelli, M.; Unterman, S. A.; Wepasnick, K. A.; McDonnell, P.; Elisseeff, J. H. Enhanced Lubrication on Tissue and Biomaterial Surfaces through Peptide-Mediated Binding of Hyaluronic Acid. *Nat. Mater.* **2014**, *13* (10), 988–995.

(12) Kayitmazer, A. B.; Koksal, A. F.; Kilic Iyilik, E. Complex Coacervation of Hyaluronic Acid and Chitosan: Effects of PH, Ionic Strength, Charge Density, Chain Length and the Charge Ratio. *Soft Matter* **2015**, *11* (44), 8605–8612.

(13) Lalevée, G.; David, L.; Montembault, A.; Blanchard, K.; Meadows, J.; Malaise, S.; Crépet, A.; Grillo, I.; Morfin, I.; Delair, T.; et al. Highly Stretchable Hydrogels from Complex Coacervation of Natural Polyelectrolytes. *Soft Matter* **2017**, *13* (37), 6594–6605.

(14) Webber, M. J.; Appel, E. A.; Meijer, E. W.; Langer, R. Supramolecular Biomaterials. *Nat. Mater.* **2015**, *15* (1), 13–26.

(15) Rosales, A. M.; Vega, S. L.; DelRio, F. W.; Burdick, J. A.; Anseth, K. S. Hydrogels with Reversible Mechanics to Probe Dynamic Cell Microenvironments. *Angew. Chemie - Int. Ed.* **2017**, *56* (40), 12132–12136.

(16) Balazs, E. A.; Cui, J. The Story of Hyaluronan Putty. *Bioact. Carbohydrates Diet. Fibre* **2013**, *2* (2), 143–151.

(17) Gibbs, D. A.; Merrill, E. W.; Smith, K. A.; Balazs, E. A. Rheology of Hyaluronic Acid. *Biopolymers* **1968**, *6* (6), 777–791.

(18) Gatej, I.; Popa, M.; Rinaudo, M. Role of the PH on Hyaluronan Behavior in Aqueous Solution. *Biomacromolecules* **2005**, *6* (1), 61–67.

(19) Wu, S.; Ai, L.; Chen, J.; Kang, J.; Cui, S. W. Study of the Mechanism of Formation of Hyaluronan Putty at PH 2 . 5 : Part I . Experimental Measurements. *Carbohydr. Polym.* **2013**, *98* (2), 1677–1682.

(20) Chakrabarti, B.; Balazs, E. A. Optical Properties of Hyaluronic Acid. Ultraviolet Circular Dichroism and Optical Rotatory Dispersion. *J. Mol. Biol.* **1973**, *78* (1), 135–141.

(21) Staskus, P. W.; Johnson, W. C. Conformational Transition of Hyaluronic Acid in Aqueous-Organic Solvent Monitored by Vacuum Ultraviolet Circular Dichroism. *Biochemistry* **1988**, *27* (5), 1522–1527.

(22) Dea, I. C.; Moorhouse, R.; Rees, D. A.; Arnott, S.; Guss, J. M.; Balazs, E. A. Hyaluronic Acid: A Novel, Double Helical Molecule. *Science* **1973**, *179* (4073), 560–562.

(23) Sheehan, J. K.; Gardner, K. H.; Atkins, E. D. T. Hyaluronic Acid: A Double-Helical Structure in the Presence of Potassium at Low PH and Found Also with the Cations Ammonium, Rubidium and Caesium. *J. Mol. Biol.* **1977**, *117* (1), 113–135.

(24) Scott, J. E.; Heatley, F. Biological Properties of Hyaluronan in Aqueous Solution Are Controlled and Sequestered by Reversible Tertiary Structures, Defined by NMR Spectroscopy. *Biomacromolecules* **2002**, *3* (3), 547–553.

(25) Blundell, C. D.; Deangelis, P. L.; Almond, A. Hyaluronan: The Absence of Amide-Carboxylate Hydrogen Bonds and the Chain Conformation in Aqueous Solution Are Incompatible with Stable Secondary and Tertiary Structure Models. *Biochem. J.* **2006**, *396* (3), 487–498.

(26) Gribbon, P.; Heng, B. C.; Hardigham, T. E. The Analysis of Intermolecular Interactions in Concentrated Hyaluronan Solutions Suggest No Evidence for Chain–chain Association. *Biochem. J.* **2000**, *350* (1), 329.

(27) Mansel, B. W.; Chu, C. Y.; Leis, A.; Hemar, Y.; Chen, H. L.; Lundin, L.; Williams, M. A. K. Zooming in: Structural Investigations of Rheologically Characterized Hydrogen-Bonded Low-Methoxyl Pectin Networks. *Biomacromolecules* **2015**, *16* (10), 3209–3216.

(28) Selig, O.; Siffels, R.; Rezus, Y. L. A. Ultrasensitive Ultrafast Vibrational Spectroscopy Employing the Near Field of Gold Nanoantennas. *Phys. Rev. Lett.* **2015**, *114* (23), 233004.

(29) Nečas, D.; Klapetek, P. Gwyddion: An Open-Source Software for SPM Data Analysis. *Central European Journal of Physics*. January 1, 2012, pp 181–188.

(30) Krężel, A.; Bal, W. A Formula for Correlating PKa Values Determined in D2O and H2O. *J. Inorg. Biochem.* **2004**, *98* (1), 161–166.

(31) De Marco, L.; Thämer, M.; Reppert, M.; Tokmakoff, A. Direct Observation of Intermolecular Interactions Mediated by Hydrogen Bonding. *J. Chem. Phys.* **2014**, *141* (3), 034502.

(32) Bodis, P.; Panman, M. R.; Bakker, B. H.; Mateo-Alonso, A.; Prato, M.; Buma, W. J.; Brouwer, A. M.; Kay, E. R.; Leigh, D. A.; Woutersen, S. Two-Dimensional Vibrational Spectroscopy of Rotaxane-Based Molecular Machines. *Acc. Chem. Res.* **2009**, *42* (9), 1462–1469.

(33) Vibrational Spectroscopy and Conformation of Peptides, Polypeptides, and Proteins. **1986**, *38*, 181–364.

(34) Woutersen, S.; Hamm, P. Time-Resolved Two-Dimensional Vibrational Spectroscopy of a Short α-Helix in Water Double-Resonance versus Pulsed Fourier Transform Two-Dimensional Infrared Spectroscopy: An Experimental and Theoretical Comparison Peptide Structure Determination by Two-Di. *J. Chem. Phys.* **2001**, *1151* (10), 2727–7733.

(35) Hamm, P.; Lim, M.; Hochstrasser, R. M. Structure of the Amide I Band of Peptides Measured by Femtosecond Nonlinear-Infrared Spectroscopy. *J. Phys. Chem. B* **1998**, *102* (31), 6123–6138.

(36) DeCamp, M. F.; DeFlores, L.; McCracken, J. M.; Tokmakoff, A.; Kwac, K.; Cho, M. Amide I Vibrational Dynamics of N-Methylacetamide in Polar Solvents: The Role of Electrostatic Interactions. *J. Phys. Chem. B* **2005**, *109* (21), 11016–11026.

(37) Cunha, A. V.; Salamatova, E.; Bloem, R.; Roeters, S. J.; Woutersen, S.; Pshenichnikov, M. S.; Jansen, T. L. C. Interplay between Hydrogen Bonding and Vibrational Coupling in Liquid N-

Methylacetamide. *J. Phys. Chem. Lett.* **2017**, *8* (11), 2438–2444.

(38) Cowman, M. K.; Spagnoli, C.; Kudasheva, D.; Li, M.; Dyal, A.; Kanai, S.; Balazs, E. A. Extended, Relaxed, and Condensed Conformations of Hyaluronan Observed by Atomic Force Microscopy. *Biophys. J.* **2005**, *88* (1), 590–602.

Figure and Legends

Figure 1: Hyaluronic acid solutions undergo a sol-gel transition in a narrow pH range. a) A tube inversion assay shows that hyaluronic acid solutions prepared at pH 1.6 exhibit viscous flow (s), whilst solutions prepared at pH 2.5 form a viscoelastic gel (p) that flows only on time scales beyond 2 min. b) The pH dependence of the viscous and elastic modulus of hyaluronic acid in heavy water solutions. We observe a sharp peak in the elastic shear modulus at pH 2.5. Inset shows that hyaluronic acid is a polymer of disaccharides, themselves composed of D-glucuronic acid and N-acetyl-D-glucosamine. c) Linear infrared spectra for hyaluronic acid solutions in D_2O at pH values ranging between 1.6 and 7. The infrared spectrum at pH=2.5 is represented by the thick solid line. Between 1550 and 1760 cm^{-1} we observe three bands: the anti-symmetric stretching mode of the carboxylate anion group, ν_{ant,COO^-}, at 1607 cm^{-1}, the amide I vibration, $\nu_{AM.I}$, at 1633 cm^{-1} and at 1726 cm^{-1} the carboxylic acid stretching mode, ν_{COOD}. The inset shows the fractions of COO^- and COOD groups determined from the IR spectra as a function of pH. Thick lines represent the expected fractions based on acid-base equilibrium equations (Supplementary Information) assuming a pK_a =2.9. We find good agreement between the measured and expected carboxylic and carboxylate fractions, with about 25% deprotonation of the carboxyl groups at pH=2.5.

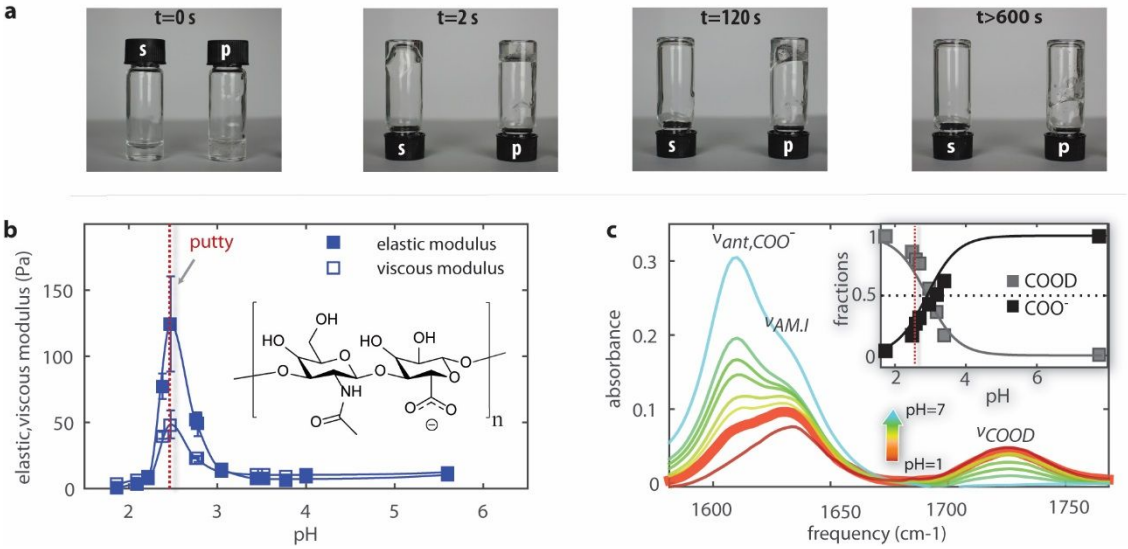

Figure 2: Isotropic two-dimensional infrared spectra of solutions of hyaluronic acid in D_2O at a concentration of 20 mg/ml in the spectral region of the carboxylic acid (ν_{COOD}) and the amide I ($\nu_{AM.I}$) vibrations. 2D IR spectra (a) for the solution state (pH=1.6), and (b) for the putty state (pH=2.5). The corresponding linear spectra are shown on the right-hand side of the 2D-IR spectra. The spectra were collected at a delay time T_w of 1.5 ps. The cross-peaks are indicated by the yellow rectangles and show the presence of vibrational interactions between $\nu_{AM.I}$ and $\nu_{COOD.}$ The thick black lines represent the integrated pump-region used for the fitting. The pump and probe spectra are centred at 1680 cm^{-1}.

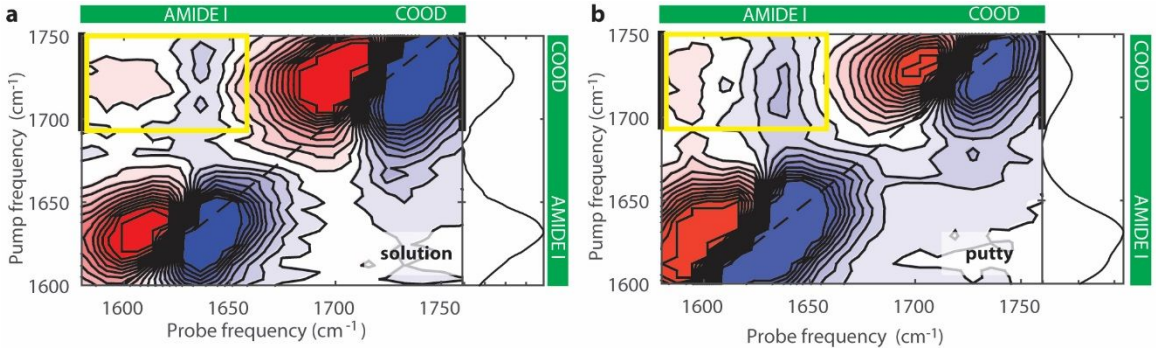

Figure 3: a) Decay traces of the cross-peak in the $\nu_{AM.I}$ vibrational region for hyaluronic acid at a concentration of 20 mg/ml in the solution and putty states. The decay traces are normalized to the carboxylic acid intensity at early time delay. The solid and dashed black lines are fits to the relaxation model (described in the Supplementary Information), for the putty and solution states, respectively. The blue lines represent the fast component: thick and dashed lines correspond, respectively, to the putty and solution states. The initial amplitude of the fast component (indicated with c_{ent}) is nearly two times larger in the putty state (c_{ent}=0.13±0.01) than in the solution state(c_{ent}=0.077±0.005). The red line represents the contribution of the slow component, whose initial amplitude c_{th} is similar between the putty and solution states ($c_{th}^{putty} \approx c_{th}^{sol.}$=0.024±0.004). Values reported are the mean and standard deviation obtained by averaging over 3 different independent measurements. b) Schematic of the relaxation model describing the cross-peak dynamics. Red and blue lines refer, respectively, to the slow component (due to thermalization) and fast component (due to energy transfer) of the cross-peak dynamics. Value shown is the average with standard deviation for 6 independent measurements.

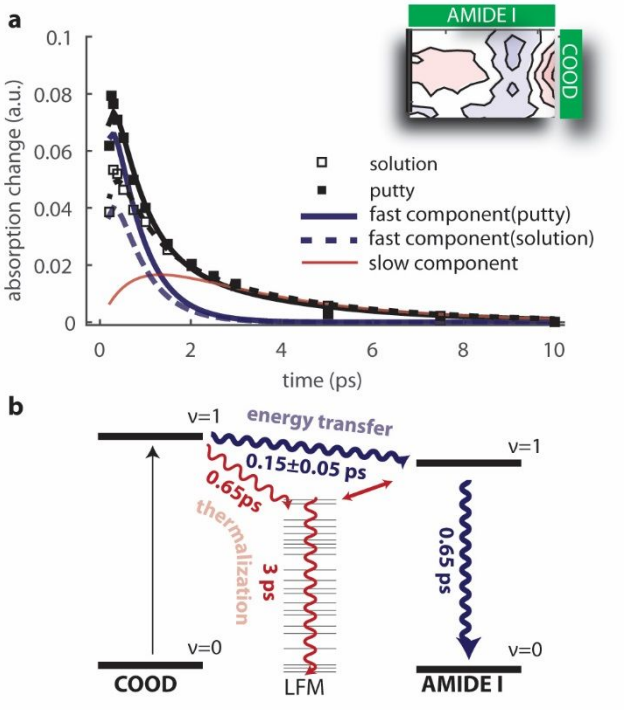

Figure 4: a) Difference 2DIR spectrum for a solution of hyaluronic acid at pH 2.5 at a concentration of 20 mg/ml. The difference 2DIR spectrum was obtained by subtracting the parallel signal from three times the perpendicular signal. The yellow rectangles indicate the cross-peak signals of the amide I and COO^- modes. b) Transient absorption spectra obtained by averaging over the pump frequency region between 1600 and 1620 cm^{-1} at pH 2.5 and 2.9, and normalized with respect to the pure anti-symmetric stretching signal of the carboxylate anion group (Fig.S10-11)

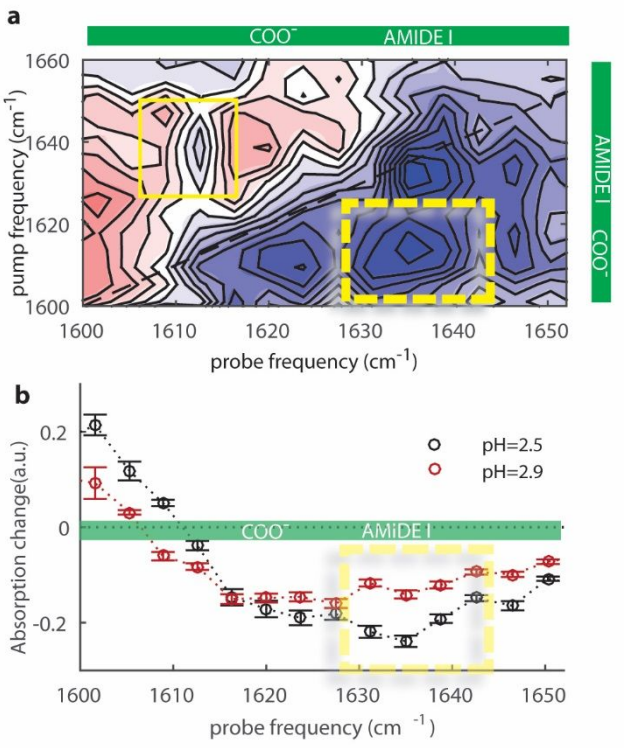

Figure 5: On the top, AFM height images of HA filaments at pH 7 and pH 2.5, respectively, colour coded from 0 nm (dark red) to 1.2 nm (white). The insets show amplitude images of smaller areas of 500x500 nm^2, indicated by the arrows. Scale bar: 500 nm. On the bottom, filament height distributions with Gaussian fits.

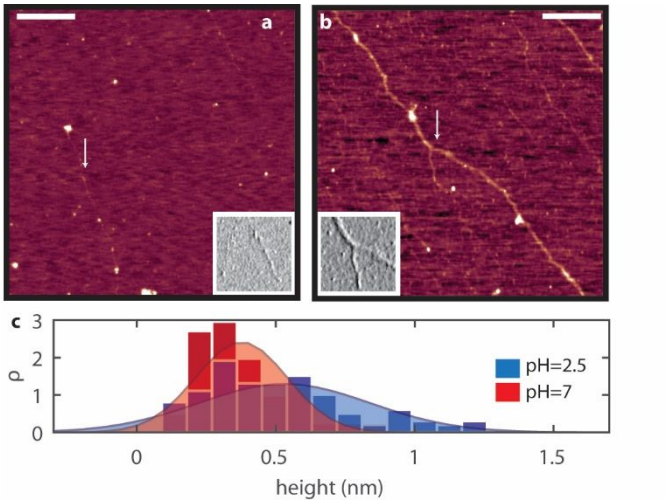

Figure 6: Schematic images showing the transition from a weakly hydrogen-bonded network of hyaluronan at pH<2.5 (top left) to a strongly hydrogen-bonded network at pH=2.5 values (right), to isolated single chains at pH>2.5 (bottom left). At pH=2.5 the balance between hydrogen-bond and Coulomb repulsion interactions is optimal, and allows the formation of hydrogen-bonds between the carboxyl acid and amide groups observed as the fast time component in the cross-peak dynamics in 2D IR. Green shaded squares indicate the formation of hydrogen-bonds between amide and protonated carboxyl groups, whilst orange shaded squares depict the formation of hydrogen-bonds between amide and deprotonated carboxyl groups.

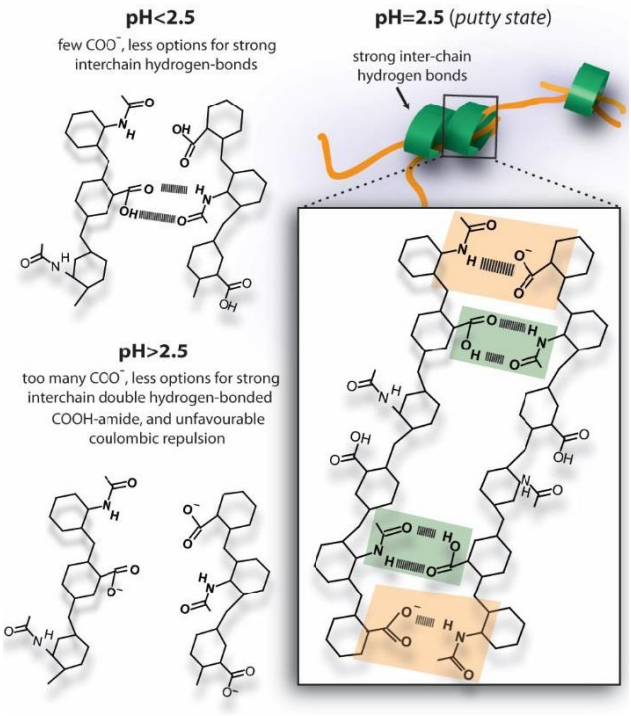

TOC figure: